

1       **Rapid tremor migration during few minute-long slow**  
2       **earthquakes in Cascadia**

3       **B. Gombert<sup>1,2</sup>, J. C. Hawthorne<sup>1</sup>**

4                   <sup>1</sup>Department of Earth Sciences, University of Oxford, U.K.

5                   <sup>2</sup>Now at Collecte Localisation Satellite, Toulouse, France

6       **Key Points:**

- 7       • Identify thousands of few-minute tremor bursts and track migration during 17 bursts  
8       • Migration speeds range from 2 to 30 m/s, with faster speeds in shorter events  
9       • Observed ruptures fill in an observational gap in the slow earthquake spectrum

---

Corresponding author: J. C. Hawthorne, [jessica.hawthorne@earth.ox.ac.uk](mailto:jessica.hawthorne@earth.ox.ac.uk)

**Abstract**

Slow earthquakes are now commonly found to display a wide range of durations, moments, and slip and propagation speeds. But not all types of slow earthquakes have been examined in detail. Here we probe tremor bursts with durations between 1 and 30 minutes, which are likely driven by few minute-long bursts of aseismic slip. We use a coherence-based technique to detect thousands of tremor bursts beneath Vancouver Island in Cascadia. Then we examine 17 of the ruptures by tracking their evolving tremor locations over an 8-km region. We find that tremor migrates at rates of 2 to 30 m/s and that shorter bursts migrate faster. The rapid propagation of the shorter bursts provides a new observation, which must be reproduced by a complete model of slow earthquakes. And though some observational biases persist, the short events' speeds appear to fill a gap in the spectrum of observed slow earthquakes. They may provide further evidence that whatever fault zone process creates slow earthquakes, it must allow for faster slip and propagation in smaller ruptures.

**Plain Language Summary**

Slow earthquakes, like earthquakes, are events with transient slip. But in slow earthquakes, faults slip slowly. Slip rates thousands or millions of times slower than in earthquakes. There are a range of types of slow earthquakes, with durations from seconds to years. But not all types of slow earthquakes have been examined in detail. Here we examine slow earthquakes with durations between 1 and 30 minutes. Specifically, we examine the small bursts of seismic energy created by the slow slip. We develop techniques used to precisely identify and locate that seismic energy, also known as tremor, and we are able to track the growth of slow earthquakes over the course of their minute-long durations. We find that during the few-minute-long events, tremor migrates at rates of 2 to 30 m/s, with fast migration in shorter events. This few-minute long migration fills an observational gap in our knowledge of slow earthquakes. The new observations may help us understand how various-duration slow earthquakes are related to each other and what causes them.

**1 Introduction**

We now frequently observe slow earthquakes with a wide range of sizes and slip rates. However, some types of slow earthquakes are recorded more often and in more detail than others. The largest slow earthquakes, known as slow slip events (SSEs), are well observed. They typically last weeks to months and can rupture several hundred km-long portions of the plate interface at subduction zones (e.g., Dragert et al., 2001; Kostoglodov et al., 2003; Obara et al., 2004; Douglas et al., 2005; Vaca et al., 2018). The slipping location in slow slip events often migrates along strike at rates of 5 to 10 km per day, and the slip rate at each location is of order  $10^{-7}$  m/s, around 100 times faster than the plate convergence rate (e.g., Miller et al., 2002; Obara & Sekine, 2009; Wech et al., 2009; Bartlow et al., 2011).

However, slow slip events are not simple, smoothly migrating ruptures. They often contain subevents: bursts of more rapid slip. In Cascadia, the longest identified subevents are several day-long intervals with more rapid slip or migration (e.g., Kao et al., 2006; Wech & Bartlow, 2014). Few hour-long subevents are also well recognised; they create rapid tremor reversals (RTRs) in Cascadia and Japan. During RTRs, tremor migrates 20 to 50 km backward along strike, through regions that have already slipped in the main event's forward migration. This reversed migration is rapid: 10 to 40 times faster than main event's forward migration (Obara, 2010; Houston et al., 2011; Yamashita et al., 2015; T. W. Thomas et al., 2013; Royer et al., 2015; Bletery et al., 2017). Geodetic data reveal that the tremor migration coincides with and is likely driven by few hour-long bursts

of accelerated aseismic slip. Slip rates are around  $10^{-6}$  m/s, an order of magnitude faster than the main event slip rate (Hawthorne et al., 2016).

Slightly shorter subevents, with durations between a few minutes and a few hours, have not yet been observed geodetically but are frequently suggested by varying tremor migration and amplitude. In Cascadia, tremor often migrates 40 to 60 km along dip during hour-long tremor streaks, moving 50 to 500 times faster than the main front (Ghosh et al., 2010). And tremor migrates up to 20 km in a range of directions during 10 to 30-minute-long rapid tremor migrations (RTMs), moving 10 to 50 times faster than the main front (Rubin & Armbruster, 2013; Peng et al., 2015; Peng & Rubin, 2016; Bletery et al., 2017). Similar 10- to 50-km-long tremor migration has also been observed in Japan, Taiwan, California, Mexico, and Alaska (e.g., Ide, 2010b; Shelly, 2010; Obara, 2012; Sun et al., 2015; Peng & Rubin, 2017). Migration rates vary among these locations, but shorter events are usually found to propagate faster.

Tremor migration has not yet been observed in detail on timescales shorter than 10 minutes, but several features of tremor suggest that complex, rapid propagation should continue to short timescales. First, tremor varies in amplitude on a range of timescales, from seconds to days (Obara, 2002; Shelly et al., 2006; Ghosh et al., 2010; Ide, 2010a), and those variations are correlated with aseismic deformation (Hawthorne & Rubin, 2013b; W. Frank, 2016). Second, some 20 to 200 second-long increases in tremor amplitude are associated with 20 to 200 second-long increases in slow slip moment rate. These moment rate increases are observable in long-period seismic data, and the 20 to 50 second-long events are called very low frequency earthquakes, or VLFs (e.g., Ito & Obara, 2006; Takeo et al., 2010; Walter et al., 2013; Hutchison & Ghosh, 2016; Maury et al., 2016; Baba et al., 2020).

In this study, we identify and analyse tremor bursts with durations between 1 and 30 minutes. Many of these events are slightly longer than VLFs but shorter than previously detected (>10-minute) tremor migrations. We first identify thousands of tremor bursts in Cascadia and then analyse 17 of them in more detail. We identify rapid tremor migration which likely reflects rapid migration of aseismic slip.

## 2 Motivation to Constrain the Spectrum of Subevents

We analyse migration on few-minute timescales for two reasons: (1) because we wish to more fully observe the range of behaviours in slow earthquakes and (2) because the range of slip speeds and behaviours could help us determine which fault zone process creates slow earthquakes. The propagation speeds of few hour-long subevents have already been used to test some models of slow earthquakes (Ariyoshi et al., 2009; Rubin, 2011; Luo & Ampuero, 2017; Luo & Liu, 2021). Some researchers have proposed that rapid subevents could reflect the rupture of asperities or asperity clusters embedded in the slow slip region. They have successfully produced the propagation speeds of few hour-subevents (RTRs) propagation speeds with a relatively simple approach: by mixing unstable patches into a region with a nominally stable slow slip rheology. The unstable patches effectively increase the local stress drop and drive more rapid slip (Ariyoshi et al., 2009; Colella et al., 2012; Peng & Rubin, 2018; Luo & Liu, 2021).

However, it may not be plausible that slip speed increases by many orders of magnitude simply because the stress drop that drives rupture increases. For many of the proposed slow slip rheologies, the stress drop required for rupture increases dramatically as the rupture speed increases (Hawthorne & Rubin, 2013c). It may be that increased local stress drops can provide enough energy to increase the rupture speed by a factor of 10 to 20, as seen in RTRs, but a factor of 100 or 1000 rupture speed increases may require a spatial variation in the *resistance* to accelerating slip.

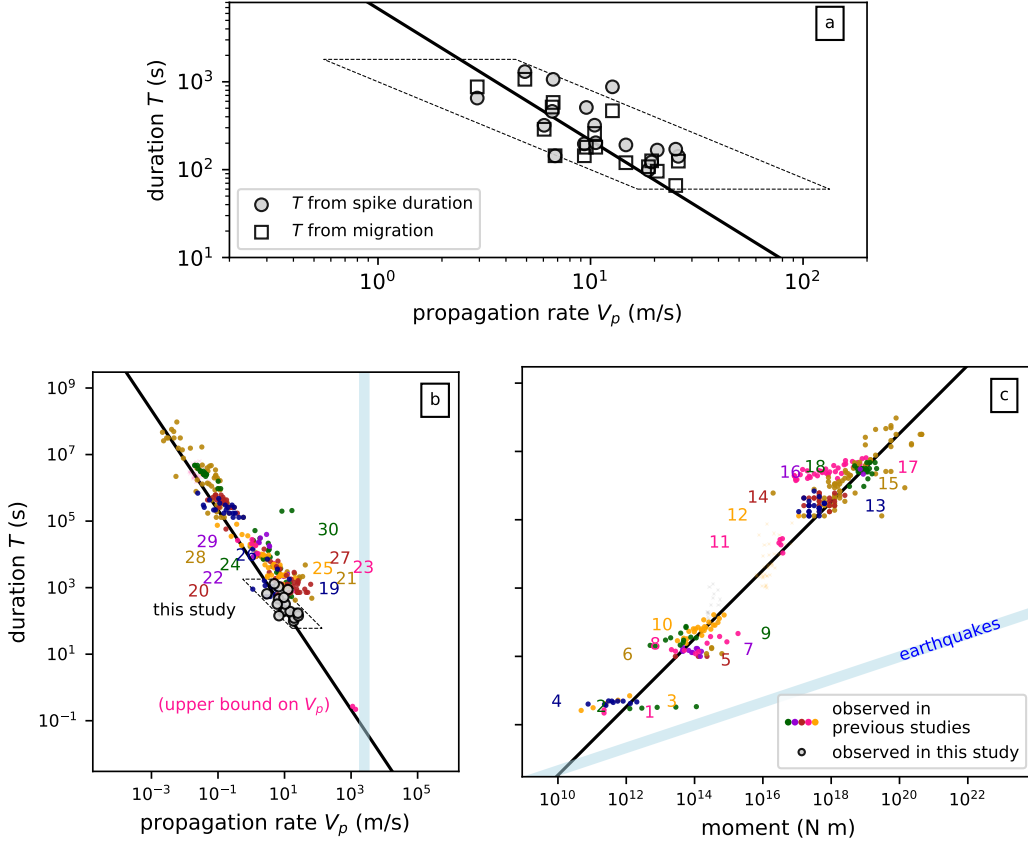


**Figure 1.** Caption on next page.

108 Such spatially variable resistance to slip is intriguing because it should not exist  
 109 for several of the proposed slow slip rheologies. For instance, if slow slip events happen  
 110 because the rheology at depth imposes a temperature-dependent speed limit (e.g., Shibazaki  
 111 & Iio, 2003; Shibazaki & Shimamoto, 2007; Hawthorne & Rubin, 2013a), that speed limit  
 112 should stay roughly the same throughout the slow slip region, where the temperature  
 113 stays relatively uniform.

114 There is, of course, already evidence that slow earthquake slip rates vary by at least  
 115 four orders of magnitude, from  $10^{-7}$  m/s in slow slip to 0.1 or 1 mm/s in VLFs and  
 116 tremor (e.g., Dragert et al., 2001; Bartlow et al., 2011; Bostock et al., 2015). However,  
 117 it remains controversial whether tremor, VLFs, and tremor bursts, are created by the  
 118 same rheology that governs slow slip slip rates. A single fault zone rheology is suggested  
 119 by a systematic trend in *observed* slow earthquakes: smaller events are faster. In Fig-  
 120 ure 1b, we plot the propagation speeds and durations of tremor bursts from a variety  
 121 of studies, and we see that shorter tremor bursts migrate faster. In Figure 1c, we plot  
 122 the moments and durations of slow earthquakes from a variety of studies, as was done  
 123 by Ide et al. (2007), and we see that observed slow earthquakes' moments  $M_0$  scale roughly  
 124 linearly with their duration  $T$ . Note that if we assume that slow earthquakes have magni-  
 125 tude-independent stress drops, as weakly suggested by observations of slow slip events, RTRs,  
 126 and LFEs (Gao et al., 2012; Hawthorne et al., 2016; Chestler & Creager, 2017), a lin-  
 127 ear moment-duration scaling implies that slip rate scales as  $M_0^{-1/2}$ . Since the linear moment-  
 128 duration trend appears to extend all the way from  $M_w$  7 slow slip events to  $M_w$  1 LFEs,



**Figure 1.** **a)** Duration versus propagation velocity for tremor bursts examined in this study. Filled circles indicate durations obtained from the widths of peaks in the  $C_p^{com}$  records while open squares indicate the durations of observable migration. The dashed parallelogram bounds the types of events we can observe with our approach. The solid black lines in panels a-c indicate a propagation rate that scales as  $T^{-1/2}$  and a moment equal to  $3 \times 10^{12}$  N-m times  $T$ . We map the line from panel c to the panels a and b assuming a rectangular rupture with a 3:1 aspect ratio and a 30-kPa stress drop. **b)** Duration vs propagation velocity and **c)** duration vs moment for our observations as well as for a selection of previous studies, indexed by the numbers below. Note that trends are visible in some studies but that there is often more uncertainty when comparing between locations. Further, to avoid clutter, we plot only a handful of observations randomly selected from each study when a large number of events are detected. Further, many authors publish only a single average propagation rate and uncertainty, or they plot a handful of figures. In those cases, we choose one or a few number from the published distribution or extract rough propagation rates from the figures. Values are taken from 1: Shelly (2017); A. M. Thomas et al. (2016); Hawthorne et al. (2019), 2: Farge et al. (2020), 3: Supino et al. (2020), 4: Bostock et al. (2015), 5: Ito et al. (2007), 6: Matsuzawa et al. (2009), 7: Maury et al. (2016), 8: Yabe et al. (2021), 9: Takeo et al. (2010), 10: Ide et al. (2008), 11: Royer et al. (2015); Hawthorne et al. (2016), 12: Itaba & Ando (2011), 13: Kitagawa et al. (2011); Itaba et al. (2013); Ochi et al. (2016), 14: Sekine et al. (2010), 15: Gao et al. (2012), 16: Rousset et al. (2017), 17: Michel et al. (2019), 18: Tu & Heki (2017), 19: Rubin & Armbruster (2013), 20: Ghosh et al. (2010), 21: Sun et al. (2015), 22: Cruz-Atienza et al. (2018), 23: Shelly (2010), 24: Peng & Rubin (2016), 25: Bletery et al. (2017), 26: Obara (2012), 27: Peng & Rubin (2017), 28: Peng et al. (2015), 29: Houston et al. (2011), and 30: Yamashita et al. (2015).

129 it would seem sensible to start assessing which rheologies would allow slip speeds that  
 130 are  $10^4$  times faster on 400-m LFE patches than on 400-km slow slip regions.

131 At this point, however, it is also sensible to recall that the scalings between mo-  
 132 ment, duration, and slip rate remain uncertain. Other moment-duration scaling have been  
 133 observed. Bostock et al. (2015) and Farge et al. (2020) inferred a very weak moment-  
 134 duration scaling, with  $T \sim M_0^0$  or  $M_0^{0.1}$ , among the low frequency earthquakes that com-  
 135 pose tremor. Michel et al. (2019) and Supino et al. (2020) identified a moment-duration  
 136 scaling similar to that seen in normal earthquakes, with  $T \sim M_0^{1/3}$  among geodetically  
 137 observed slow slip events and among sub-second tremor bursts, respectively. Further, the  
 138 linear moment-duration trend identified by Ide et al. (2007) depends on connecting days  
 139 to months-long slow slip events and seconds-long LFEs and VLFs (Figure 1c). And there  
 140 are significant gaps along that trend. We now have abundant observations of sub-second  
 141 LFEs, 10-second VLFs, and days to months-long slow slip events, but there are fewer  
 142 observations between those durations, and there may be missing observations that fall  
 143 off the trend (Gomberg et al., 2016).

144 To overcome all the observational gaps, we will require a wide range of approaches.  
 145 For instance, recent work has suggested an expansion of the tremor band to longer du-  
 146 rations (Kaneko et al., 2018; Masuda et al., 2020). Here we focus on a different band and  
 147 attempt to expand the range of slow slip subevents to shorter durations: between 2 and  
 148 10 minutes. We modify our tremor detection methodology to search for the expected short,  
 149 rapid migration on these timescales, and we partly fill the apparent gap in the duration-  
 150 propagation rate trend (Figure 1b). We note, however, that our approach still suffers from  
 151 observational bias; it was not designed to find events that are much faster or slower than  
 152 the along-trend speeds.

153 In the sections that follow, we first describe our phase coherence-based tremor de-  
 154 tection approach (section 3) and the available data and processing (section 4). Then we  
 155 describe the observed large-scale tremor migration patterns in section 5, examine small-  
 156 scale tremor migration in 17 tremor bursts in section 6, and discuss the migrations' im-  
 157 plications in section 7.

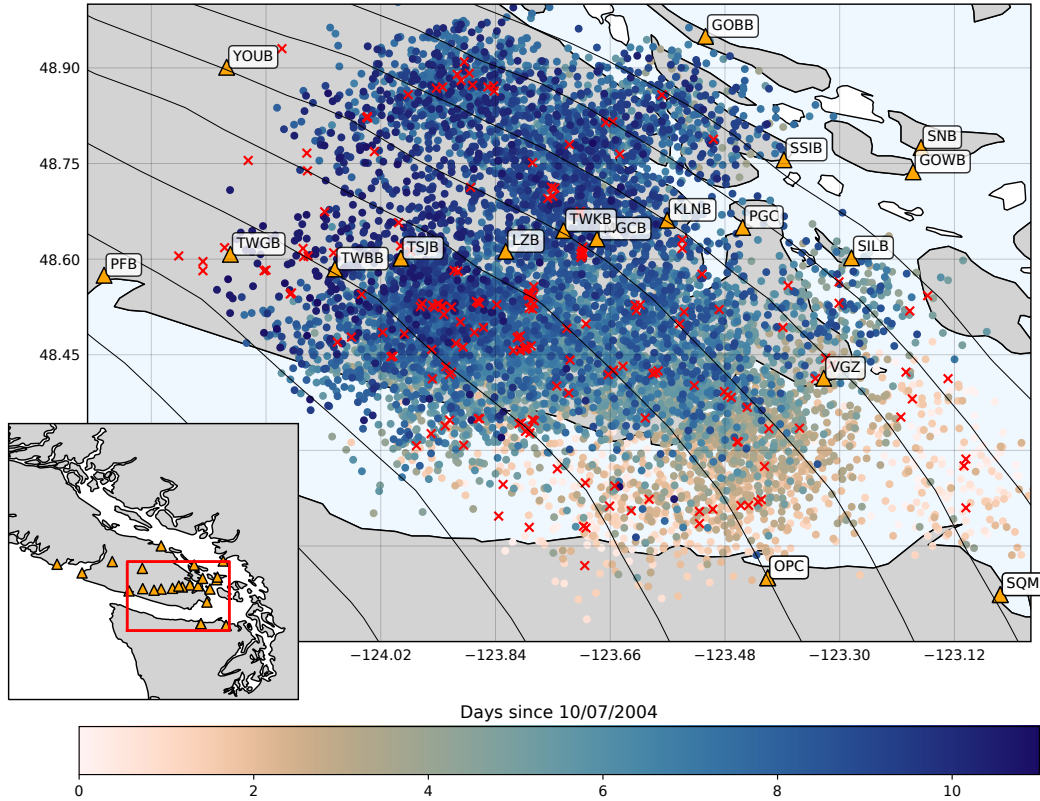


**Figure 2.** Map of study area. Orange triangles are the seismic stations used in 2004. Red crosses are the 130 LFEs locations from (Bostock et al., 2012). Circles mark spikes in inter-component coherence, coloured by time. They are plotted at random locations within 5 km of the template LFE used in the coherence calculation. Black lines are the 30 to 44-km depth contours from McCrory et al. (2012), spaced every 2 km.

### 158 **3 Tremor Detection Method: Identifying Tremor Near Template Lo-** 159 **cations**

160 To identify and locate tremor, we use a phase coherence-based approach developed  
 161 by Hawthorne & Ampuero (2017), which is a variant of empirical matched field techniques  
 162 (e.g., Bucker, 1976; Harris & Kvaerna, 2010; Corciulo et al., 2012; Wang et al., 2015).  
 163 This approach allows us to identify tremor that ruptures fault patches close to known  
 164 low frequency earthquakes (LFEs). The coherence calculation is able to identify tremor  
 165 even if the tremor ruptures are complex or if the tremor consists of a series of ruptures,  
 166 as the method combines two common approaches to identifying tremor. First, as inspired  
 167 by matched filter techniques (Brown et al., 2008; Bostock et al., 2012; W. B. Frank et  
 168 al., 2014; Shelly, 2017), the calculation compares seismograms between events. It assesses  
 169 whether the template and target signals could have the same Green's functions: if they  
 170 result from the same source-station path. Second, as inspired by cross-station techniques

171 (Armbruster et al., 2014; Peng et al., 2015; Savard & Bostock, 2015), the calculation com-  
 172 pares seismograms between stations or components. It assesses whether the signals at  
 173 all stations or components could result from the same tremor source time functions.

### 174 3.1 Inter-Station Coherence

In all of the coherence calculations, we begin with a set of template seismograms  $d_{tkm}$  that were created by Bostock et al. (2012) and which represent the signals generated by LFEs occurring at 130 locations on the plate interface (red crosses in Figure 2). The LFEs are recorded at a range of stations  $k$  and on three components  $m$  (east, north, and up). We compare the template seismograms at each station with 30 to 60-second-long intervals of target seismic data ( $d_{dkm}$ ). To assess whether a 30 or 60-second interval contains tremor coming from the same location as the template, we compute the inter-station phase coherence at a range of frequencies  $f$ :

$$C_p^{sta}(f) = \frac{1}{3} \sum_{m=1}^3 \frac{2}{N(N-1)} \sum_{k=1}^N \sum_{l=k+1}^N \operatorname{Re} \left[ \frac{\hat{d}_{dkm} \hat{d}_{tkm}^* \hat{d}_{dlm}^* \hat{d}_{tlm}}{|\hat{d}_{dkm} \hat{d}_{tkm} \hat{d}_{dlm} \hat{d}_{tlm}|} \right]. \quad (1)$$

175 Here  $\hat{d}_{tkm}(f)$  and  $\hat{d}_{dkm}(f)$  are the Fourier transforms of the template and target data  
 176 at station  $k$  and component  $m$ , and we compare between stations  $k$  and  $l$  in each term.  
 177 There are  $N$  stations in total, and we average over the  $N(N-1)/2$  station pairs and  
 178 over the three components at each station. Note that we have dropped the frequency in-  
 179 dexing on the right hand side for readability, and we also average over frequencies  $f$  be-  
 180 tween 1 and 6 Hz.

Note that if the target seismograms  $d_{dkm}$  record tremor from the same location as the template seismograms, then the template and target seismograms may be written as  $\hat{d}_{tkm} = \hat{s}_t \hat{g}_{km}$  and  $\hat{d}_{dkm} = \hat{s}_d \hat{g}_{km}$ , where  $\hat{s}_t$  and  $\hat{s}_d$  are the template and target tremor source time functions,  $\hat{g}_{km}$  is the path effect, and  $C_p^{sta}$  becomes

$$C_p^{sta}(f) = \frac{1}{3} \sum_{m=1}^3 \frac{2}{N(N-1)} \sum_{k=1}^N \sum_{l=k+1}^N \operatorname{Re} \left[ \frac{(\hat{s}_t \hat{g}_{km})(\hat{s}_d^* \hat{g}_{km}^*)(\hat{s}_t \hat{g}_{lm})(\hat{s}_d^* \hat{g}_{lm}^*)}{|\hat{s}_t \hat{s}_d \hat{g}_{km} \hat{g}_{lm}|^2} \right] = 1. \quad (2)$$

181 So by identifying intervals with high phase coherence  $C_p^{sta}$ , near 1, we can identify in-  
 182 tervals when tremor is occurring at the same location as previously located templates.  
 183 Synthetic tests suggest that  $C_p^{sta}$  is significantly larger than zero only when tremor oc-  
 184 curs within about 0.5 km from the template: within a fraction of one seismic wavelength  
 185 (Figure S3).

### 186 3.2 Inter-Component Coherence

In some cases, however, we do not need or want 0.5-km precision. We simply wish to know whether tremor is occurring in *roughly* the same area as the template: within 10 km or so. In such situations, we compute an inter-component phase coherence:

$$C_p^{com}(f) = \frac{1}{N} \sum_{k=1}^N \frac{2}{3(3-1)} \sum_{m=1}^3 \sum_{n=m+1}^3 \operatorname{Re} \left[ \frac{\hat{d}_{dkm} \hat{d}_{tkm}^* \hat{d}_{dkn} \hat{d}_{tkn}}{|\hat{d}_{dkm} \hat{d}_{tkm} \hat{d}_{dkn} \hat{d}_{tkn}|} \right]. \quad (3)$$

187 Here we multiply the Fourier domain seismograms across components  $m$  and  $n$  rather  
 188 than across stations  $k$ . Then we average over component pairs and over stations.

To understand why  $C_p^{com}$  is often high even when the target tremor is slightly off-set from the template, note that when the tremor is close to the template, its Green's functions are likely to have shapes similar to the template's Green's function. The tremor Green's functions  $g'_{km}(t)$  may simply be time-shifted versions of the template Green's functions  $g_{km}(t)$ . They may be approximated by  $g'_{km} = g_{km}(t - \Delta t)$ , where the time

shift  $\Delta t$  results from the difference in travel time to the source. Now we may note that if we have multiple recording on the same station, just at different components  $m$  and  $n$ , the change in travel time  $\Delta t$  will remain the same. If we input tremor with these shifted Green's functions into the phase coherence calculation in equation (3), we eliminate the travel time change and obtain

$$C_p^{com}(f) = \frac{1}{N} \sum_{k=1}^N \frac{2}{3(3-1)} \sum_{m=1}^3 \sum_{n=m+1}^3 \operatorname{Re} \left[ \frac{(\hat{s}_t \hat{g}_{km})(\hat{s}_d^* \hat{g}_{km}^* e^{-i2\pi f \Delta t})(\hat{s}_t^* \hat{g}_{kn}^*)(\hat{s}_d \hat{g}_{kn} e^{i2\pi f \Delta t})}{|\hat{s}_t \hat{s}_d \hat{g}_{km} \hat{g}_{kn}|^2} \right] = 1. \quad (4)$$

189 Here  $s_t$  and  $s_d$  are the source time functions of the template and tremor signals, respec-  
190 tively.

191 It is of course difficult to know whether the Green's functions' shapes remain the  
192 same over broad regions. We find empirically that the Green's functions retain a sim-  
193 ilar enough shape for detection even as tremor locations change by 10 to 20 km; we ob-  
194 tain high  $C_p^{com}$  when the inter-station  $C_p^{sta}$  calculations for nearby templates imply that  
195 tremor is located up to 10 or 20 km away from the template.

#### 196 4 Templates, Data, and Processing

197 In our initial approach to the data, we compute the phase coherence  $C_p^{sta}$  and  $C_p^{com}$   
198 between each template and the seismic data recorded during 13 to 20 day-long intervals  
199 during four major slow slip events in 2004, 2008, 2009, and 2010. The 130 LFE templates  
200 created by Bostock et al. (2012) are located beneath the southern tip of Vancouver Is-  
201 land and the Juan de Fuca Strait, at depths ranging from 28 to 45 km (crosses in Fig-  
202 ure 2).

203 We use data from stations in permanent and temporary seismic networks, includ-  
204 ing the Canadian National Seismograph Network ((**alias?**)), the POLARIS-BC Network  
205 (PO; Nicholson et al., 2005), the Plate Boundary Observatory Borehole Seismic Network  
206 ((**alias?**)), the Pacific Northwest Seismic Network ((**alias?**)), and the USArray Trans-  
207 portable Array ((**alias?**)). The available networks and stations evolved between the dif-  
208 ferent slow slip events. Stations from the POLARIS-BC network were available only dur-  
209 ing the 2004 event while the PBO stations are available only after 2008. The POLARIS-  
210 BC network is ideal for this study, thanks to its dense configuration across the south-  
211 ern half of Vancouver Island, and Figure 2 shows the stations used for the 2004 slow slip  
212 event. Maps and tables of the 2008, 2009 and 2010 networks are available in Figure S1  
213 and Table T1.

214 To prepare the data, we filter the target and template seismograms to between 0.6 Hz  
215 and 20 Hz and downsample to a common sampling rate of 40 Hz. We extract a portion  
216 of each template, from 0.2 s before to 4.8 s after a manually picked S-wave arrival and  
217 then compute the coherences  $C_p^{sta}$  and  $C_p^{com}$  between these template segments and a set  
218 of overlapping 60 second-long windows of target data, starting every 6 s.

219 Further details of the  $C_p$  calculations are as described by Hawthorne & Ampuero  
220 (2017), but to summarise, we first cross-correlate at each station in the time domain, com-  
221 puting  $d_{dkm} \cdot d_{tkm}$ . Then we taper the time domain correlation with a Hanning filter,  
222 convert to the frequency domain, compute  $C_p$ , and average  $C_p$  over frequencies between  
223 1 and 6 Hz.

#### 224 5 Observed Large-Scale Tremor Patterns

225 Figure 3 shows 10 days of  $C_p^{sta}$  and  $C_p^{com}$  during the 2004 slow slip event for two  
226 different templates (#246 and #12), about 40 km one from another. During the first days  
227 analyzed, tremor has not yet reached Vancouver Island. The calculated phase coherence

228 is scattered around 0, and no high values stand out. The amplitude of the scatter in  $C_p$   
 229 depends on noise in the template used and on the number of available stations. With  
 230 the stations available in 2004, standard deviations in  $C_p^{sta}$  are between 0.007 and 0.05,  
 231 and standard deviations in  $C_p^{com}$  are between 0.015 and 0.036.

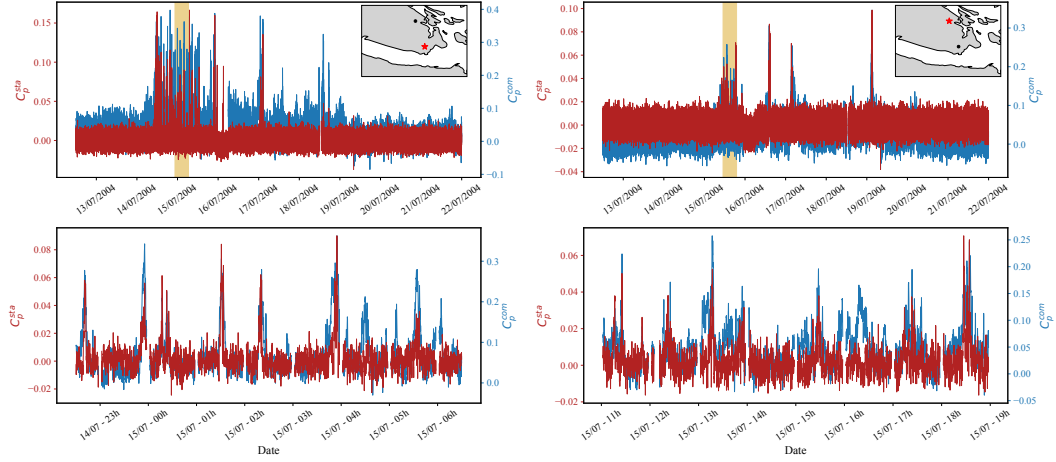


**Figure 3. Phase coherence time series for two templates in 2004. a-b)** 10 days-long time series of the inter-station phase coherence ( $C_p^{sta}$ , red) and the inter-component phase coherence ( $C_p^{com}$ , blue). The red star in each inset shows the location of the associated template. The orange bands delimit the time period shown in c-d. **c-d)** An expanded view of 8 hours of the time series shown in a) and b), respectively.

232 When the main slow slip front reaches the locations of the templates, the coher-  
 233 ence values begin to spike to values well above noise-induced variability. The templates  
 234 in Figure 3 see the main front arrival on the 14<sup>th</sup> and 15<sup>th</sup> July, respectively, and have  
 235  $C_p^{com}$  values that reach 0.38 and  $C_p^{sta}$  values that reach 0.17. However, the coherence val-  
 236 ues are not continuously high. The activity is fragmented into 1 to 30 minute-long spikes  
 237 separated by intervals of low coherence that last minutes to hours. The spikes associ-  
 238 ated with the templates in Figure 3 can be seen in more detail in the 8 hour-long win-  
 239 dows in panels c and d, but similar spikes in coherence are observed for all 130 templates  
 240 examined in this study. The most intense sequence of spikes typically lasts 1 to 2 days,  
 241 while the main front passes, but spikes in coherence can be seen for up to five days.

242 The spikes in the phase coherence  $C_p^{sta}$  and  $C_p^{com}$  are presumably created by bursts  
 243 of tremor occurring on the plate interface. The inter-component coherence  $C_p^{com}$  is ideal  
 244 for identifying and measuring the duration of these bursts, as  $C_p^{com}$  seems to remain high  
 245 even when tremor spreads to locations as far as 10 to 20 km from a given template. In  
 246 contrast, the inter-station coherence  $C_p^{sta}$  decreases when the tremor is offset by more  
 247 than a fraction of the seismic wavelength. The difference in inter-component and inter-  
 248 station tremor detection is apparent for a number of spikes for template #246 (Figure 3a  
 249 and c). For instance, the spike at 3:45 on the 15<sup>th</sup> July is longer on the  $C_p^{com}$  time se-  
 250 ries, and the spike at 4:30 on the 15<sup>th</sup> July is observable only the  $C_p^{com}$  time series.

We use a simple peak detection algorithm included in SciPy to identify a number of spikes in each  $C_p^{com}$  time series. Proposed spikes are identified as maxima in  $C_p^{com}$  when

$$C_{p,k}^{com} \geq \alpha \times \sigma_{C_{p,k}}, \quad (5)$$

251 where  $\sigma_{C_{p,k}}$  the standard deviation of the phase coherence during a time before tremor  
 252 begins, and  $\alpha$  is a factor between 2.0 and 3.5. The beginning and end of the spikes are

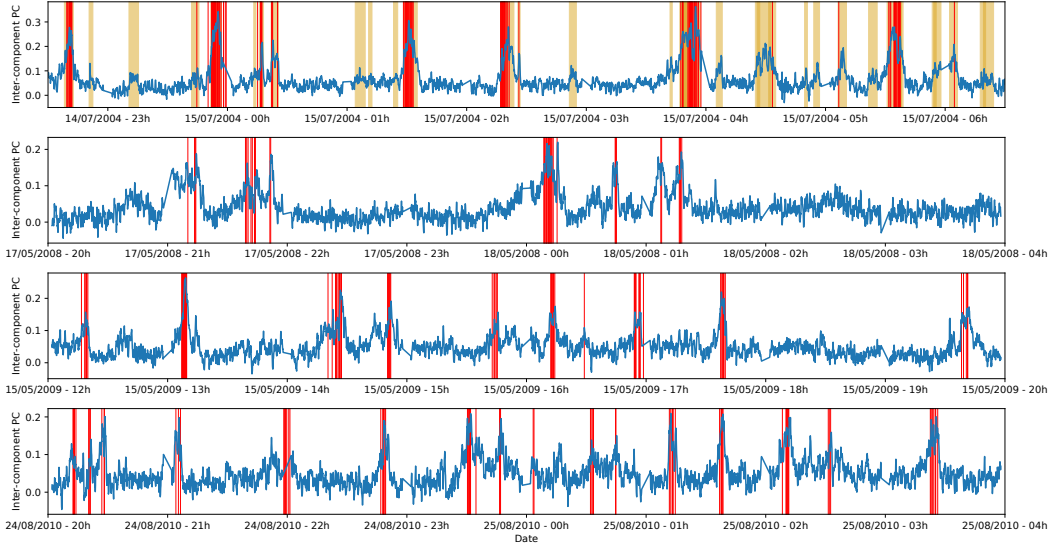


**Figure 4.**  $C_p^{com}$  over multiple slow slip events. Inter-component phase coherence  $C_p^{com}$  with template LFE #246, for time intervals in (a) 2004, (b) 2008, (c) 2009, and (d) 2010. Red lines mark the timing of LFE detections from (Bostock et al., 2015). Yellow bands on the top plot show identified spikes in the  $C_p^{com}$  time series, requiring that peaks are at least with  $\alpha = 3.0$  times the standard deviation.

253 the times when  $C_p^{com}$  decreases to half its maximum value, and we accept spikes that  
 254 last at least 60 seconds. Depending on the threshold  $\alpha$ , we detect between 22,000 and  
 255 86,000 events in 2004. Several spikes are delineated in yellow in Figure 4a. Catalogues  
 256 of the spikes are provided as a supplementary file, and Figure S7 shows the distribution  
 257 of spike durations for different values of  $\alpha$ . Note that because we use a 60-second win-  
 258 dow for our coherence calculations,  $C_p^{com}$  is smoothed on that timescale, and the dura-  
 259 tions of shorter spikes may be overestimated.

260 Figure 2 shows the spatio-temporal distribution of tremor bursts detected with  $\alpha =$   
 261 3.0. Each burst is plotted at a random location within 5 km of the associated template  
 262 location and are colored by time. The bursts track the along-strike propagation of the  
 263 main ETS front in 2004, from the Juan de Fuca Strait on the 10<sup>th</sup> July to  $\sim$ 90 km north-  
 264 west of the Strain on the 19<sup>th</sup> July (e.g., Wech et al., 2009; Bostock et al., 2015).

265 We can also compare our results directly with the LFE detections of Bostock et  
 266 al. (2015). Vertical red lines in Figure 4 mark LFE detections with the relevant template.  
 267 The matched filter detections in the catalogue coincide remarkably well with times of  
 268 high phase coherence. All LFE detections occur within intervals of high  $C_p^{com}$ , though  
 269 a few intervals of high  $C_p^{com}$  do not include a LFE detection. The lack of LFE detections  
 270 in some high  $C_p^{com}$  intervals may arise because tremor is coming from an adjacent part  
 271 of the fault or because the tremor time series is complex, so that it is difficult to sepa-  
 272 rate overlapping LFEs with a matched filter approach.

273 We observe similar tremor burst spacing and migration patterns for the 2008, 2009,  
 274 and 2010 slow slip events (Figure S1). 8 hour-long  $C_p^{com}$  time series from the four events  
 275 can be compared in Figure 4, though we focus on the 2004 results in this study because  
 276 the  $C_p$  time series have the highest resolution in 2004, when the POLARIS seismic net-  
 277 work was running on Vancouver Island.



## 6 Tremor Burst Propagation

### 6.1 One Example

Our observed spikes in  $C_p^{com}$ , along with tremor spikes seen in previous work (Ghosh et al., 2009; Rubin & Armbruster, 2013; Bostock et al., 2015), suggest that much of the tremor in Cascadia occurs in short bursts. Here we seek to probe the bursts in more detail: to examine the shape and migration some of the shorter bursts.

We track the spatial and temporal evolution of 17 tremor bursts that are visible as well-resolved spikes in the  $C_p^{com}$  record. We identify a high-quality template that records each burst and then define a circular grid of potential tremor locations around that template, as illustrated in Figure 5a. Each grid is 8 km in diameter and is inclined along the slab interface identified by McCrory et al. (2012). In order to track tremor within the grid, we note that tremor coming from each of the possible locations is likely to have a Green’s function whose shape is similar to the template’s Green’s function. We verify that similarity by comparing the waveforms of closely spaced template LFEs; the waveforms of templates located about 5 km apart have similar shapes (see Figure S2).

We shift the timing of the template seismograms to reflect the variation in the source-station travel time among the grid locations. The travel time for each location is computed using a uniform shear wave velocity model. We have estimated the apparent shear wave velocity for each LFE template by plotting the variation in 3-D distance from the LFE to the various stations against the arrival time for each station. We observe a linear relationship between distance and travel time, suggesting that a uniform velocity model is sufficient for our analysis. Tests with a layered velocity model and ray path calculations achieved similar results.

Once we have time-shifted the template waveforms for a given location, we compute the inter-station phase coherence  $C_p^{sta}$  to determine when tremor occurs at that location. Figure 5 shows snapshots of the coherence during one three minute-long burst. During this time, the region of high phase coherence migrates about 1.6 km at a speed around 30 km/hr. The tremor moves from southeast to northwest, roughly along the strike of the subduction zone. This northwestward migration is pulse-like; the first location stops generating tremor before the last location generates tremor.

### 6.2 Propagation for 17 Tremor Bursts

Tremor migration is also well-resolved for 16 other analysed bursts, with migration durations between 60 and 1100 seconds. Some of these are illustrated in flipbooks M1 to M6 in the supplementary material. To more precisely characterise the tremor migration speed in each burst, we select a profile across the grid parallel to its propagation direction and identify the front position (Figure S4). We then compute a linear regression between the propagating front position and time to obtain the propagation velocity (Figure S5). The 17 analysed bursts and their propagation speeds are listed in Table T2. Figure 1a shows the relationship between the bursts’ duration  $T$  and the propagation velocity  $V_r$  of the 17 events.

We cannot be sure that the observed duration-propagation velocity relationship is representative of the general population of tremor bursts, as we did not choose the bursts to be analysed in a systematic way. We determined tremor location in several tens of bursts with high  $C_p^{com}$  values and identified those with clear migration. Nevertheless, it is interesting to note that among the 17 events analysed, shorter events propagate faster. The minute-long events propagate at more than 20 m/s, while the 15 minute-long events propagate at only  $\sim 4$  m/s.

The faster propagation of shorter bursts persists for two definitions of burst duration. The open squares in Figure 1a indicate the durations of visually identified tremor

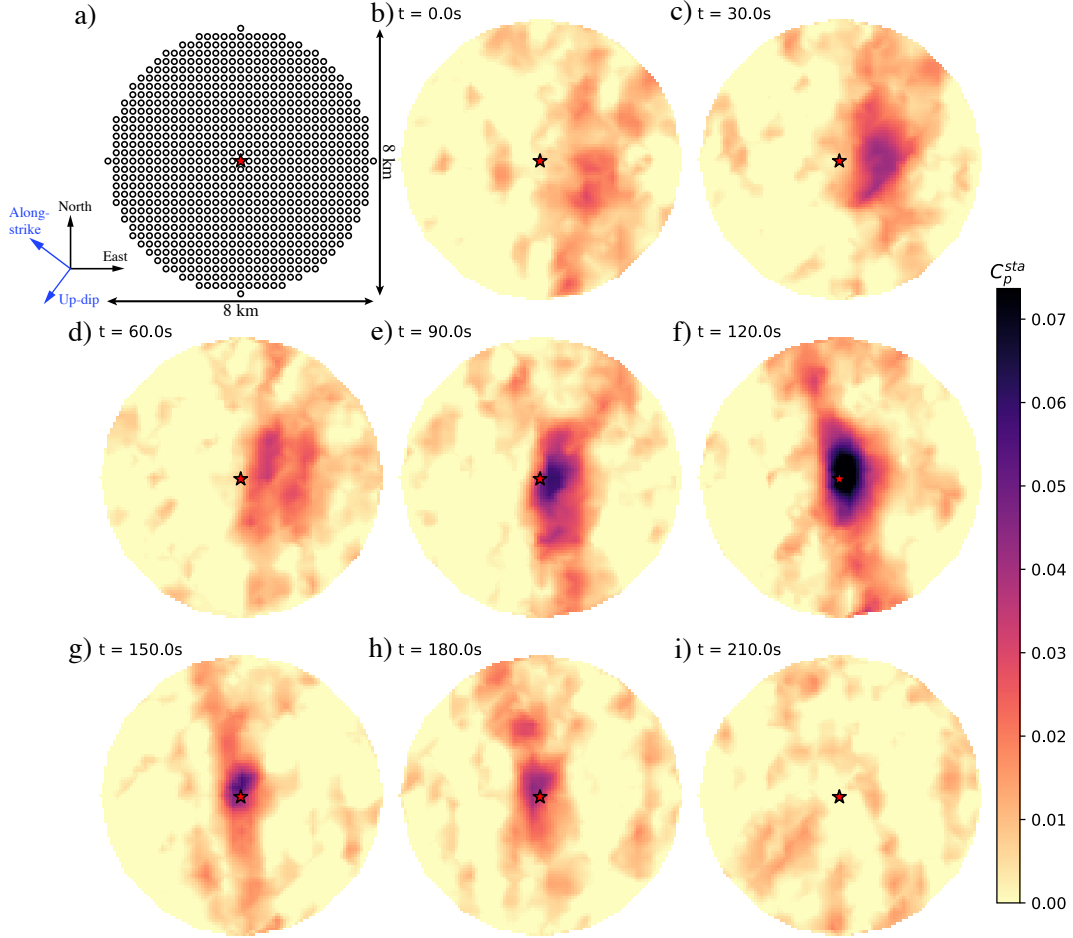


**Figure 5.** Grid search for tremor during a burst detected at template #181. **a)** Grid configuration and dimensions. **b-i)** Snapshots of  $C_p^{sta}$  computed for each point on the grid shown in **a** and interpolated. Indicated times are the middle of one-minute-long window used to compute the phase coherence. Red stars mark the location of the LFE used as template. In this example, the slow-slip propagates roughly 1.6 km at 9.2 m/s.

327 migration while the the filled circles indicate durations estimated from the  $C_p^{com}$  time  
 328 series: when  $C_p^{com}$  is above a local background value. This latter definition of duration  
 329 is likely to be more accurate, as the tremor could migrate out of the 8-km grid where  
 330 we computed  $C_p^{sta}$ , and the inter-component phase coherence  $C_p^{com}$  can identify at least  
 331 some tremor in a broader region.

### 332 6.3 Range of Observable Propagation Velocities

333 Before we interpret the observed durations and propagation velocities, however, it  
 334 is important to note that we have chosen our methodology to examine a particular range  
 335 of tremor bursts: those with durations between 1 and 30 minutes and propagation ex-  
 336 tents between 1 and 8 km. This range of observable speeds and durations is outlined with  
 337 a dashed line in Figure 1a.

338 We cannot identify migration over distances less than 1 km because of the reso-  
 339 lution of the phase coherence calculations given 1-6 Hz seismic data from 5 to 10 sta-



340 tions. To map the potential smearing of the high coherence region for a given template,  
 341 we create a synthetic signal for each point on the circular grid by time-shifting the tem-  
 342 plate waveforms. Then we compute  $C_p^{sta}$  between those synthetics and the unshifted tem-  
 343 plate seismograms. Some of the noisier template seismograms allow for elongate smear-  
 344 ing of the high  $C_p^{sta}$  over 3 km-long distances (Figure S3c and d). However, we have looked  
 345 for tremor propagation only with the higher-quality templates, which show relatively cir-  
 346 cular smearing of high  $C_p^{sta}$  over smaller regions, with half-width of around 0.5 km (Fig-  
 347 ure S3a and b). These resolution tests imply that we should be able to identify tremor  
 348 that propagates around 1 km or more.

349 We cannot identify migration over distances larger 8 km because that migration  
 350 would extend outside the 8 km-wide grid around the relevant template LFEs, and we  
 351 have not developed the technique to map migration from the area around one LFE tem-  
 352 plate to another. This 8-km limit constrains the open squares to fall below the upper  
 353 diagonal dashed line in Figure 1a. However, synthetic tests imply if there were rapid prop-  
 354 agation in larger events, we could have identified at least a few km of that propagation  
 355 (Figure S6). And the filled circles can in principle plot up to a factor of 2 above the 8-  
 356 km line, as they indicate durations taken from spikes in the  $C_p^{com}$  record. Comparisons  
 357 of  $C_p^{com}$  and  $C_p^{sta}$  suggest that  $C_p^{com}$  can remain high when tremor is within 10 or 20 km  
 358 of the template.

359 The roughly 1 to 8 km constraints suggest that we would observe an anticorrela-  
 360 tion between burst duration and propagation speed even for a collection of bursts with  
 361 random properties. However, the durations and propagation speeds we observe do not  
 362 seem to fill the box of observable values; they are more consistent with the  $T^{-1/2}$  trend  
 363 that one would expect for slow earthquakes whose moments scale linearly with duration.  
 364 It thus seems likely that our observed duration-propagation speed anticorrelation is real—  
 365 not entirely an observational artefact, but since we did not choose the 17 bursts to anal-  
 366 yse rigorously, we cannot be sure.

## 367 7 Discussion

368 We have used a high-precision, coherence-based technique to identify numerous bursts  
 369 of tremor. We mapped tremor migration over 1 to 6 km in 17 bursts with durations be-  
 370 tween 1 and 22 minutes. The tremor migrates at speeds of 4 to 20 m/s, moving more  
 371 quickly in shorter bursts. The sub-ten minute, rapidly migrating bursts represent a new  
 372 observation. They are yet another category of slow earthquakes that must be reproduced  
 373 by any complete physical model of subduction zone slip.

### 374 7.1 Pulse-Like Ruptures

375 If we assume, as seems plausible, that the observed migration of tremor results from  
 376 a migrating location of aseismic slip, it is interesting to note that the propagation of tremor  
 377 is pulse-like rather than crack-like; the locations slipping early in the bursts (e.g., brighter  
 378 portions of Figure 5b and c) stop slipping before slip occurs at later locations (e.g., in  
 379 Figure 5g and h). Such pulse-like migration of tremor and slip is also apparent in the  
 380 main slow slip events in Cascadia, as well as in some longer tremor bursts (Dragert et  
 381 al., 2001; Wech et al., 2009; Ghosh et al., 2010; Royer et al., 2015).

382 Pulse-like ruptures can appear unintuitive because slip at later locations should in-  
 383 crease the stress at the initial locations, and that stress increase has the potential to drive  
 384 slip. The pulse-like ruptures could indicate that the slow slip region has a particular type  
 385 of rheology: one that allows a rapid recovery in stress as the slip rate slows, so that the  
 386 initial location can accommodate an increasing stress as it slows down but other parts  
 387 of the fault accelerate (Heaton, 1990; Zheng & Rice, 1998; Lu et al., 2007; Noda et al.,  
 388 2009; Bizzarri, 2010). Alternatively, the pulse-like ruptures could indicate that the subevent

389 rupture is constrained to an elongate region. Slip may migrate along the long axis of that  
 390 region, and the initial slipping location may stop slipping because it has slipped enough  
 391 relative to its short-axis edges to accommodate the local stress drop. Slip at the far end  
 392 of the rupture may produce an insignificant stress change at the initial location (e.g., Hawthorne  
 393 & Rubin, 2013a; Michel et al., 2017; Dal Zilio et al., 2020).

394 However, pulse-like ruptures are unlikely in some models of slow slip. One of the  
 395 first proposed explanations of slow slip suggests that slow slip regions have a "standard,"  
 396 potentially unstable, velocity-weakening rheology but that the regions have a particu-  
 397 lar size; they may be large enough to accelerate but too small to reach seismic slip speeds  
 398 (Y. J. Liu & Rice, 2005, 2007; Rubin, 2008; Li et al., 2018; Romanet et al., 2018). But  
 399 most simulations of those size-limited slow slip ruptures appear more crack-like than pulse-  
 400 like, at least in a visual inspection (Y. J. Liu & Rice, 2005; Rubin, 2008). A more rig-  
 401 orous investigation of the slip rate profiles in these models would help us further assess  
 402 whether fault sizes and geometry alone can explain slow slip events.

## 403 7.2 Too Fast to Be Driven by a Change in Stress Drop?

404 We may also investigate the rheology of the slow slip region by addressing their speed:  
 405 how can 5-minute-long subevents propagate 200 times faster than the main slow slip front?  
 406 Do the subevents have a greater driving stress drop and thus a larger strain energy re-  
 407 lease, or do they have a lower resistance to acceleration: a smaller fracture energy? To  
 408 partially address this question, we may note that the strain energy released in an elon-  
 409 gate rupture normally scales as  $\Delta\tau^2W$ : as the stress drop  $\Delta\tau$  squared times the rupture  
 410 width  $W$  (e.g., Lawn, 1993). This strain energy must equal the fracture energy dissipated  
 411 by the rupture, which is a function of the rheology, the initial conditions, and the slip  
 412 rate. Most of the complex rheologies proposed to explain slow slip have fracture ener-  
 413 gies that increase dramatically as the slip rate increases. The strong increase in resis-  
 414 tance with slip rate keeps the slip rates low. A factor of 200 increase in slip rate, as seems  
 415 plausible for our fastest events, is likely to require at least a factor of 10 increase in frac-  
 416 ture energy in a shear-induced dilatancy model (L. Liu et al., 2010; Segall et al., 2010)  
 417 and at least a factor of 5 increase in fracture energy in a model with a velocity-strengthening  
 418 transition (Hawthorne & Rubin, 2013a,c). Our subevents have widths  $W$  at least fac-  
 419 tor of 10 narrower than the main slow slip region, so for their slip to supply such an in-  
 420 creased fracture energy, they would need stress drops at least 7 times larger than the main  
 421 event stress drop. We do not have stress drops estimates for our subevents, but geode-  
 422 tic and tremor count-based analyses for half- to few-hour events suggest that subevent  
 423 stress drops are comparable to or smaller than the main event stress drop (Rubin & Arm-  
 424 bruster, 2013; Hawthorne et al., 2016; Bletery et al., 2017).

425 Some modelers have produced locally high stress drops and slip rates by mixing  
 426 unstable patches into a mostly stable slow slip region (Ariyoshi et al., 2009, 2012; Colella  
 427 et al., 2012; Peng & Rubin, 2018; Luo & Liu, 2021). However, these patch-driven mod-  
 428 els have focused on slightly slow tremor fronts and have so far allowed propagation rates  
 429 less than 10 to 50 times faster than the main front (Ariyoshi et al., 2012; Colella et al.,  
 430 2012; Peng & Rubin, 2018). It remains to be seen whether patch-driven models can al-  
 431 low the higher propagation rates seen here and observed by Ghosh et al. (2010), particu-  
 432 larly in ruptures that are just a few km wide.

433 If they cannot, it may be worth considering whether the slow slip rheology varies  
 434 with time, perhaps because the pore pressure changes, (Rubin, 2011; Peng & Rubin, 2017)  
 435 or whether fault properties vary in space to allow locally reduced resistance to high slip  
 436 rates and thus faster ruptures.

437

### 7.3 Potential Consistency With a Slow Earthquake Continuum

438

439

440

441

442

443

444

445

446

447

448

449

450

451

452

453

454

455

It would be particularly interesting to consider spatially variable fault properties if we knew that a single fault zone process produced the entire range of slow earthquakes, from slow slip events to tremor LFEs (Ide et al., 2007). Some rheologies proposed to explain slow slip are unlikely to produce very wide-ranging slip rates, particularly if slip speeds increase as ruptures get smaller. For instance, a rheology where slip rate depends on temperature rather than patch size is unlikely to allow slip rates that increase by a factor of 10,000 as patches get smaller (Shibazaki & Iio, 2003; Matsuzawa et al., 2010; Hawthorne & Rubin, 2013c). Size-limited models, where slip rates tend to be 10 to 100 times the driving slip rate (Y. J. Liu & Rice, 2005, 2007; Rubin, 2008; Skarbek et al., 2012; Wei et al., 2018), may also be unlikely to produce very high slip rates. The apparently faster slip in smaller events could indicate that whatever process generates slip in slow earthquakes, it depends on some size-dependent fault property. For instance, fault zone width might be smaller on smaller fault segments, allowing shorter fluid diffusion times and faster slip in dilatancy models (Marone et al., 1990; Lockner & Byerlee, 1994; Segall & Rice, 1995; Segall et al., 2010; L. Liu et al., 2010; Y. Liu, 2013), or smaller patches could have high concentrations of brittle asperities that drive rapid viscous deformation (Lavie et al., 2013; Fagereng et al., 2014; Behr et al., 2018; Goswami & Barbot, 2018; Behr & Bruggmann, 2021).

456

457

458

459

A range of observations have suggested that we should consider these size-dependent fault properties. Smaller observed slow earthquakes tend to be faster (see Figure 1 and e.g., Ide et al., 2007; Gao et al., 2012), and the statistics of observed slip are consistent with a continuum of slip rates (Ide, 2008; Ide & Maury, 2018; Hawthorne & Bartlow, 2018).

460

461

462

463

464

465

466

467

468

469

Our identified subevents results may provide further evidence that slow earthquakes constitute a continuum with size-dependent slip rates. We find that smaller tremor bursts are faster, and our observed propagation velocities and durations fall along the trends defined by previously observed slow earthquakes, as shown in Figure 1b. The match with previous observations is not perfect, but the mismatch could result from observational bias in tremor detection. Our results are restricted by the methodology to a size range between 1 and 8 km, and some others' results are also restricted. The RTRs and slow slip fronts identified by Houston et al. (2011) and Bletery et al. (2017) are constrained to be longer than 10 km because they used tremor with location spacing or accuracy of 5 to 10 km.

470

471

472

473

474

475

476

477

478

479

480

481

Our propagation rates are difficult to directly compare with the linear moment-duration scaling found by Ide et al. (2007). However, we can roughly compare the two by plotting black lines in each panel of Figure 1, which assume that (1) slow earthquake moments scale linearly with duration, with a moment rate of  $3 \times 10^{12} \text{ N m s}^{-1}$ , and (2) slow earthquakes have magnitude-independent stress drops  $\Delta\tau$  around 30 kPa, as is consistent with a few observations but remains poorly constrained (Schmidt & Gao, 2010; Rubin & Armbruster, 2013; Hawthorne et al., 2016; Bletery et al., 2017; Chestler & Creager, 2017; A. M. Thomas et al., 2018). We assume elliptical ruptures with uniform stress drop and a 3:1 aspect ratio, and we estimate the propagation velocity by dividing the length of the ellipse by the rupture duration. The comparison suggests that our propagation rates also fall roughly along the trend defined by observed slow earthquakes' moments and durations.

482

### 7.4 Potential Inconsistency With a Slow Earthquake Continuum

483

484

485

486

487

However, it is too early to firmly infer that all slow earthquakes are governed by the same fault zone processes. Our results fill one observational gap, but other gaps in the slow earthquake spectrum remain, and we have not addressed observed scalings that differ from the overall trend in Figure 1c (Bostock et al., 2015; Gomberg et al., 2016; Michel et al., 2019; Farge et al., 2020; Supino et al., 2020).

488 Further, one could interpret our observed propagation velocities as evidence against  
 489 a simple continuum of slow earthquakes. The events we analyse are slightly slower than  
 490 one would expect after extrapolating the propagation velocities of tremor fronts iden-  
 491 tified by Bletery et al. (2017) and (Houston et al., 2011) (Figure 1b). One could argue  
 492 that there are slow earthquakes with a wide range of propagation rates and durations,  
 493 located all over the plot in Figure 1b. Our and others' identified events could simply have  
 494 sizes that reflect our observational capabilities (Gomberg et al., 2016).

495 Such observational bias does not seem to explain all the trends in the observed events'  
 496 sizes. For instance, by extracting durations from the  $C_p$  time series and propagation from  
 497 the tremor locations, we should be able to identify at least part of the propagation in  
 498 longer, faster events, even if they are 20 km across. And if 30-s-long  $M_W$  5 earthquakes  
 499 were common, it would be surprising that they have not yet been spotted. But it may  
 500 also be surprising, at least to our physical intuition, that a single fault zone process could  
 501 create slow earthquakes with wide-ranging slip rates, so we must be careful to remem-  
 502 ber that many events could go unobserved.

## 503 8 Conclusions

504 We have identified thousands of short bursts of tremor beneath Vancouver Island  
 505 by employing a phase coherence method developed by Hawthorne & Ampuero (2017)  
 506 and set of template LFE waveforms created by Bostock et al. (2012). For seventeen bursts,  
 507 we perform a grid search on the fault plane to track the evolution of tremor and likely  
 508 slip. We find that these minutes-long events have pulse-like ruptures. They move 1 to  
 509 6 km at speeds of 3 m/s to 25 m/s. Smaller events tend to be faster, and the events' prop-  
 510 erties fall roughly, though not quite on, the duration-propagation velocity trend defined  
 511 by previously observed events. These trends provide further, albeit still inconclusive, ev-  
 512 idence that slow earthquakes with a wide range of slip rates are created by the same fault  
 513 zone processes. In any case, they indicate that any complete physical model of slow slip  
 514 in Cascadia should reproduce not just events that last weeks, with propagation rates of  
 515 0.1 m/s, and subevents that last 3 hours, with propagation rates of 5 m/s, but also subevents  
 516 that last 2 minutes, with propagation rates of 20 m/s.

## 517 9 Open Research

518 The tremor catalogues created in this study are in the process of being uploaded  
 519 to a National Geoscience Data Centre repository, hosted by the British Geological Sur-  
 520 vey. The catalogues are temporarily available at the link below.

<https://drive.google.com/drive/folders/1HhDKhwUdfymJR01tgTJMYXE0GdI03pu?usp=sharing>

521 The facilities of IRIS Data Services, and specifically the IRIS Data Management  
 522 Center, were used for access to waveforms, related metadata, and/or derived products  
 523 used in this study. IRIS Data Services are funded through the Seismological Facilities  
 524 for the Advancement of Geoscience and EarthScope (SAGE) Proposal of the National  
 525 Science Foundation under Cooperative Agreement EAR-1261681. To identify peaks in  
 526 coherence, we used the *find\_peaks()* function of the Scipy python package (Jones et al.,  
 527 2001–).

## 528 Acknowledgments

529 We thank M. Bostock for providing the LFE catalogue and waveforms and J. Cas-  
 530 sidy for his help with missing data during the 2008 ETS. This study was funded by NERC  
 531 standard grant NE/P012507/1.

532

**References**

533

Ariyoshi, K., Hori, T., Ampuero, J.-P., Kaneda, Y., Matsuzawa, T., Hino, R., & Hasegawa, A. (2009). Influence of interaction between small asperities on various types of slow earthquakes in a 3-D simulation for a subduction plate boundary. *Gondwana Res.*, *16*(3-4), 534–544. doi: 10.1016/j.gr.2009.03.006

536

537

Ariyoshi, K., Matsuzawa, T., Ampuero, J.-P., Nakata, R., Hori, T., Kaneda, Y., . . . Hasegawa, A. (2012). Migration process of very low-frequency events based on a chain-reaction model and its application to the detection of preseismic slip for megathrust earthquakes. *Earth Planets Space*, *64*(8), 693–702. doi: 10.5047/eps.2010.09.003

538

539

540

541

542

Armbruster, J. G., Kim, W.-Y., & Rubin, A. M. (2014). Accurate tremor locations from coherent S and P waves. *J. Geophys. Res.*, *119*(6), 5000–5013. doi: 10.1002/2014JB011133

543

544

545

Baba, S., Takeo, A., Obara, K., Matsuzawa, T., & Maeda, T. (2020). Comprehensive detection of very low frequency earthquakes off the Hokkaido and Tohoku Pacific coasts, northeastern Japan. *J. Geophys. Res.*, *125*(1). doi: 10.1029/2019JB017988

546

547

548

549

Bartlow, N. M., Miyazaki, S., Bradley, A. M., & Segall, P. (2011). Space-time correlation of slip and tremor during the 2009 Cascadia slow slip event. *Geophys. Res. Lett.*, *38*, L18309. doi: 10.1029/2011GL048714

550

551

552

Behr, W. M., & Brgmann, R. (2021). Whats down there? The structures, materials and environment of deep-seated slow slip and tremor. *Philosophical Transactions of the Royal Society A: Mathematical, Physical and Engineering Sciences*, *379*(2193), 20200218. doi: 10.1098/rsta.2020.0218

553

554

555

556

Behr, W. M., Kotowski, A. J., & Ashley, K. T. (2018). Dehydration-induced rheological heterogeneity and the deep tremor source in warm subduction zones. *Geology*, *46*(5), 475–478. doi: 10.1130/G40105.1

557

558

559

Bizzarri, A. (2010). Pulse-like dynamic earthquake rupture propagation under rate-, state- and temperature-dependent friction. *Geophys. Res. Lett.*, *37*, L18307. doi: 10.1029/2010GL044541

560

561

562

Bletery, Q., Thomas, A. M., Hawthorne, J. C., Skarbek, R. M., Rempel, A. W., & Krogstad, R. D. (2017). Characteristics of secondary slip fronts associated with slow earthquakes in Cascadia. *Earth Planet. Sci. Lett.*, *463*, 212–220. doi: 10.1016/j.epsl.2017.01.046

563

564

565

566

Bostock, M. G., Royer, A. A., Hearn, E. H., & Peacock, S. M. (2012). Low frequency earthquakes below southern Vancouver Island. *Geochem., Geophys., Geosyst.*, *13*(11), Q11007. doi: 10.1029/2012GC004391

567

568

569

Bostock, M. G., Thomas, A. M., Savard, G., Chuang, L., & Rubin, A. M. (2015). Magnitudes and moment-duration scaling of low-frequency earthquakes beneath southern Vancouver Island. *J. Geophys. Res.*, *120*(9), 6329–6350. doi: 10.1002/2015JB012195

570

571

572

573

Brown, J. R., Beroza, G. C., & Shelly, D. R. (2008). An autocorrelation method to detect low frequency earthquakes within tremor. *Geophys. Res. Lett.*, *35*(16), L16305. doi: 10.1029/2008GL034560

574

575

576

Bucker, H. P. (1976). Use of calculated sound fields and matchedfield detection to locate sound sources in shallow water. *J. Acoust. Soc. Amer.*, *59*(2), 368–373. doi: 10.1121/1.380872

577

578

579

Chestler, S. R., & Creager, K. C. (2017). Evidence for a scale-limited low-frequency earthquake source process. *J. Geophys. Res.*, *122*(4), 3099–3114. doi: 10.1002/2016JB013717

580

581

582

Colella, H. V., Dieterich, J. H., Richards-Dinger, K., & Rubin, A. M. (2012). Complex characteristics of slow slip events in subduction zones reproduced in multi-cycle simulations. *Geophys. Res. Lett.*, *39*(20), L20312. doi: 10.1029/2012GL053276

583

584

585



- 586 Corciulo, M., Roux, P., Campillo, M., Dubucq, D., & Kuperman, W. (2012). Mul-  
587 tiscale matched-field processing for noise-source localization in exploration geo-  
588 physics. *GEOPHYSICS*, *77*(5), KS33–KS41. doi: 10.1190/geo2011-0438.1
- 589 Cruz-Atienza, V. M., Villafuerte, C., & Bhat, H. S. (2018). Rapid tremor migration  
590 and pore-pressure waves in subduction zones. *Nat. Comm.*, *9*. doi: 10.1038/s41467-  
591 018-05150-3
- 592 Dal Zilio, L., Lapusta, N., & Avouac, J. (2020). Unraveling scaling properties of  
593 slowslip events. *Geophys. Res. Lett.*, *47*(10). doi: 10.1029/2020GL087477
- 594 Douglas, A., Beavan, J., Wallace, L., & Townend, J. (2005). Slow slip on the north-  
595 ern Hikurangi subduction interface, New Zealand. *Geophys. Res. Lett.*, *32*, 16305.
- 596 Dragert, H., Wang, K. L., & James, T. S. (2001). A silent slip event on the deeper  
597 Cascadia subduction interface. *Science*, *292*(5521), 1525–1528. doi: 10.1126/  
598 science.1060152
- 599 Fagereng, ., Hillary, G. W. B., & Diener, J. F. A. (2014). Brittle-viscous deforma-  
600 tion, slow slip, and tremor. *Geophys. Res. Lett.*, *41*(12), 4159–4167. doi: 10.1002/  
601 2014GL060433
- 602 Farge, G., Shapiro, N. M., & Frank, W. B. (2020). Moment-  
603 duration scaling of Low-Frequency Earthquakes in Guerrero, Mex-  
604 ico. *J. Geophys. Res.*, *n/a*(n/a), 2019JB019099. (preprint:  
605 <https://agupubs.onlinelibrary.wiley.com/doi/pdf/10.1029/2019JB019099>) doi:  
606 10.1029/2019JB019099
- 607 Frank, W. (2016). Slow slip hidden in the noise: The intermittence of tectonic re-  
608 lease. *Geophys. Res. Lett.*, *43*. doi: 10.1002/2016GL069537
- 609 Frank, W. B., Shapiro, N. M., Husker, A. L., Kostoglodov, V., Romanenko, A., &  
610 Campillo, M. (2014). Using systematically characterized low-frequency earth-  
611 quakes as a fault probe in Guerrero, Mexico. *J. Geophys. Res.*, *119*(10), 7686–  
612 7700. doi: 10.1002/2014JB011457
- 613 Gao, H., Schmidt, D. A., & Weldon, R. J. (2012). Scaling relationships of source  
614 parameters for slow slip events. *Bull. Seis. Soc. Amer.*, *102*(1), 352–360. doi: 10  
615 .1785/0120110096
- 616 Geological Survey of Canada. (1989). *Canadian National Seismograph Network.*  
617 *International Federation of Digital Seismograph Networks. Dataset / seismic net-*  
618 *work.* doi: <https://doi.org/10.7914/SN/CN>
- 619 Ghosh, A., Vidale, J. E., Sweet, J. R., Creager, K. C., & Wech, A. G. (2009).  
620 Tremor patches in Cascadia revealed by seismic array analysis. *Geophys. Res.*  
621 *Lett.*, *36*, L17316. doi: 10.1029/2009GL039080
- 622 Ghosh, A., Vidale, J. E., Sweet, J. R., Creager, K. C., Wech, A. G., Houston, H.,  
623 & Brodsky, E. E. (2010). Rapid, continuous streaking of tremor in Cascadia.  
624 *Geochem., Geophys., Geosyst.*, *11*, Q12010. doi: 10.1029/2010GC003305
- 625 Gomberg, J., Wech, A., Creager, K., Obara, K., & Agnew, D. (2016). Reconsid-  
626 ering earthquake scaling. *Geophys. Res. Lett.*, *43*(12), 6243–6251. doi: 10.1002/  
627 2016GL069967
- 628 Goswami, A., & Barbot, S. (2018). Slow-slip events in semi-brittle serpentinite fault  
629 zones. *Scientific Reports*, *8*(1), 6181. doi: 10.1038/s41598-018-24637-z
- 630 Harris, D. B., & Kvaerna, T. (2010). Superresolution with seismic arrays using em-  
631 pirical matched field processing. *Geophys. J. Intern.*, *182*(3), 1455–1477. doi: 10  
632 .1111/j.1365-246X.2010.04684.x
- 633 Hawthorne, J. C., & Ampuero, J.-P. (2017). A phase coherence approach to identify-  
634 ing co-located earthquakes and tremor. *Geophys. J. Intern.*, *209*(2), 623–642. doi:  
635 10.1093/gji/ggx012
- 636 Hawthorne, J. C., & Bartlow, N. M. (2018). Observing and modeling the spec-  
637 trum of a slow slip event. *J. Geophys. Res.*, *123*(5), 4243–4265. doi: 10.1029/  
638 2017JB015124
- 639 Hawthorne, J. C., Bostock, M. G., Royer, A. A., & Thomas, A. M. (2016). Varia-

- 640 tions in slow slip moment rate associated with rapid tremor reversals in Cascadia.  
641 *Geochem., Geophys., Geosyst.*, *17*(12), 4899–4919. doi: 10.1002/2016GC006489
- 642 Hawthorne, J. C., & Rubin, A. M. (2013a). Laterally propagating slow slip events in  
643 a rate and state friction model with a velocity-weakening to velocity-strengthening  
644 transition. *J. Geophys. Res.*, *118*(7), 3785–3808. doi: 10.1002/jgrb.50261
- 645 Hawthorne, J. C., & Rubin, A. M. (2013b). Short-time scale correlation between  
646 slow slip and tremor in Cascadia. *J. Geophys. Res.*, *118*(3), 1316–1329. doi: 10  
647 .1002/jgrb.50103
- 648 Hawthorne, J. C., & Rubin, A. M. (2013c). Tidal modulation and back-  
649 propagating fronts in slow slip events simulated with a velocity-weakening to  
650 velocity-strengthening friction law. *J. Geophys. Res.*, *118*(3), 1216–1239. doi:  
651 10.1002/jgrb.50107
- 652 Hawthorne, J. C., Thomas, A. M., & Ampuero, J.-P. (2019). The rupture extent of  
653 low frequency earthquakes near Parkfield, CA. *Geophys. J. Intern.*. doi: 10.1093/  
654 gji/ggy429
- 655 Heaton, T. H. (1990). Evidence for and implications of self-healing pulses of slip  
656 in earthquake rupture. *Physics of the Earth and Planetary Interiors*, *64*(1), 1–20.  
657 doi: 10.1016/0031-9201(90)90002-F
- 658 Houston, H., Delbridge, B. G., Wech, A. G., & Creager, K. C. (2011). Rapid tremor  
659 reversals in Cascadia generated by a weakened plate interface. *Nat. Geosci.*, *4*(6),  
660 404–409. doi: 10.1038/ngeo1157
- 661 Hutchison, A. A., & Ghosh, A. (2016). Very low frequency earthquakes spa-  
662 tiotemporally asynchronous with strong tremor during the 2014 episodic tremor  
663 and slip event in Cascadia. *Geophys. Res. Lett.*, *43*(13), 6876–6882. doi:  
664 10.1002/2016GL069750
- 665 Ide, S. (2008). A Brownian walk model for slow earthquakes. *Geophys. Res. Lett.*,  
666 *35*(17), L17301. doi: 10.1029/2008GL034821
- 667 Ide, S. (2010a). Quantifying the time function of nonvolcanic tremor based on a  
668 stochastic model. *J. Geophys. Res.*, *115*, B08313. doi: 10.1029/2009JB000829
- 669 Ide, S. (2010b). Striations, duration, migration and tidal response in deep tremor.  
670 *Nature*, *466*(7304), 356–359. doi: 10.1038/nature09251
- 671 Ide, S., Beroza, G. C., Shelly, D. R., & Uchide, T. (2007). A scaling law for slow  
672 earthquakes. *Nature*, *447*(7140), 76–79. doi: 10.1038/nature05780
- 673 Ide, S., Imanishi, K., Yoshida, Y., Beroza, G. C., & Shelly, D. R. (2008). Bridging  
674 the gap between seismically and geodetically detected slow earthquakes. *Geophys.*  
675 *Res. Lett.*, *35*(10), L10305. doi: 10.1029/2008GL034014
- 676 Ide, S., & Maury, J. (2018). Seismic moment, seismic energy, and source dura-  
677 tion of slow earthquakes: Application of brownian slow earthquake model to  
678 three major subduction zones. *Geophys. Res. Lett.*, *45*(7), 3059–3067. doi:  
679 10.1002/2018GL077461
- 680 IRIS Transportable Array. (2003). *USArray transportable array. International Fed-*  
681 *eration of Digital Seismograph Networks. Dataset / seismic network.* doi: [https://](https://doi.org/10.7914/SN/TA)  
682 [doi.org/10.7914/SN/TA](https://doi.org/10.7914/SN/TA)
- 683 Itaba, S., & Ando, R. (2011). A slow slip event triggered by teleseismic surface  
684 waves. *Geophys. Res. Lett.*, *38*(21), L21306. doi: 10.1029/2011GL049593
- 685 Itaba, S., Kitagawa, Y., Koizumi, N., Takahashi, H., Matsumoto, N., Takeda, N., ...  
686 Shiomi, K. (2013). *Short-term slow slip events in the Tokai area, the Kii Penin-*  
687 *sula and the Shikoku District, Japan (from November 2012 to April 2013)* (Report  
688 of the Coordinating Committee for Earthquake Prediction No. 90).
- 689 Ito, Y., & Obara, K. (2006). Very low frequency earthquakes within accretionary  
690 prisms are very low stress-drop earthquakes. *Geophys. Res. Lett.*, *33*, L09302. doi:  
691 10.1029/2006GL025883
- 692 Ito, Y., Obara, K., Shiomi, K., Sekine, S., & Hirose, H. (2007). Slow earthquakes co-  
693 incident with episodic tremors and slow slip events. *Science*, *315*(5811), 503–506.

- 694       doi: 10.1126/science.1134454
- 695 Jones, E., Oliphant, T., Peterson, P., et al. (2001–). *SciPy: Open source scientific*  
696 *tools for Python*. Retrieved from <http://www.scipy.org/> ([Online; accessed {to-  
697 day}]])
- 698 Kaneko, L., Satoshi, I., & Nakano, M. (2018). Slow earthquakes in the microseism  
699 frequency band (0.11.0 hz) off Kii Peninsula, Japan. *Geophys. Res. Lett.*, *45*(6),  
700 2618–2624. doi: 10.1002/2017GL076773
- 701 Kao, H., Shan, S.-J., Dragert, H., Rogers, G., Cassidy, J. F., Wang, K., . . . Ra-  
702 machandran, K. (2006). Spatial-temporal patterns of seismic tremors in northern  
703 Cascadia. *J. Geophys. Res.*, *111*, B03309. doi: 10.1029/2005JB003727
- 704 Kitagawa, Y., Itaba, S., Koizumi, N., Takahashi, M., Matsumoto, N., & Takeda,  
705 N. (2011). *The variation of the strain, tilt and groundwater level in the Shikoku*  
706 *District and Kii Peninsula, Japan (from November 2010 to May 2011)* (Report of  
707 the Coordinating Committee for Earthquake Prediction No. 86).
- 708 Kostoglodov, V., Singh, S. K., Santiago, J. A., Franco, S. I., Larson, K. M., Lowry,  
709 A. R., & Bilham, R. (2003). A large silent earthquake in the Guerrero seismic  
710 gap, Mexico. *Geophys. Res. Lett.*, *30*(15), 1807. doi: 10.1029/2003GL017219
- 711 Lavier, L. L., Bennett, R. A., & Duddu, R. (2013). Creep events at the brittle duc-  
712 tile transition. *Geochem., Geophys., Geosyst.*, *14*(9), 3334–3351. doi: 10.1002/ggge  
713 .20178
- 714 Lawn, B. (1993). *Fracture of Brittle Solids* (2nd ed.). Cambridge,UK: Cambridge  
715 University Press.
- 716 Li, H., Wei, M., Li, D., Liu, Y., Kim, Y., & Zhou, S. (2018). Segmentation of slow  
717 slip events in south central Alaska possibly controlled by a subducted oceanic  
718 plateau. *J. Geophys. Res.*, *123*(1), 2017JB014911. doi: 10.1002/2017JB014911
- 719 Liu, L., Gurnis, M., Seton, M., Saleeby, J., Muller, R. D., & Jackson, J. M. (2010).  
720 The role of oceanic plateau subduction in the Laramide orogeny. *Nat. Geosci.*,  
721 *3*(5), 353–357. doi: 10.1038/ngeo829
- 722 Liu, Y. (2013). Numerical simulations on megathrust rupture stabilized under strong  
723 dilatancy strengthening in slow slip region. *Geophys. Res. Lett.*, *40*(7), 1311–1316.  
724 doi: 10.1002/grl.50298
- 725 Liu, Y. J., & Rice, J. R. (2005). Aseismic slip transients emerge spontaneously in  
726 three-dimensional rate and state modeling of subduction earthquake sequences. *J.*  
727 *Geophys. Res.*, *110*, B08307. doi: 10.1029/2004JB003424
- 728 Liu, Y. J., & Rice, J. R. (2007). Spontaneous and triggered aseismic deformation  
729 transients in a subduction fault model. *J. Geophys. Res.*, *112*(B9), B09404. doi:  
730 10.1029/2007JB004930
- 731 Lockner, D. A., & Byerlee, J. D. (1994). Dilatancy in hydraulically isolated faults  
732 and the suppression of instability. *J. Geophys. Res.*, *21*(22), 2353–2356. doi: 10  
733 .1029/94GL02366
- 734 Lu, X., Lapusta, N., & Rosakis, A. J. (2007). Pulse-like and crack-like ruptures in  
735 experiments mimicking crustal earthquakes. *Proceedings of the National Academy*  
736 *of Sciences*, *104*(48), 18931–18936. doi: 10.1073/pnas.0704268104
- 737 Luo, Y., & Ampuero, J.-P. (2017). Tremor migration patterns and the collective be-  
738 havior of deep asperities mediated by creep. *EarthArXiv*. doi: 10.17605/OSF.IO/  
739 MBCAV
- 740 Luo, Y., & Liu, Z. (2021). Fault zone heterogeneities explain depth-dependent pat-  
741 tern and evolution of slow earthquakes in Cascadia. *Nat. Comm.*, *12*(1), 1959. doi:  
742 10.1038/s41467-021-22232-x
- 743 Marone, C., Raleigh, C. B., & Scholz, C. H. (1990). Frictional behavior and con-  
744 stitutive modeling of simulated fault gouge. *J. Geophys. Res.*, *95*(B5), 7007–7025.  
745 doi: 10.1029/JB095iB05p07007
- 746 Masuda, K., Ide, S., Ohta, K., & Matsuzawa, T. (2020). Bridging the gap between  
747 low-frequency and very-low-frequency earthquakes. *Earth, Planet. Space*, *72*(1),



47. doi: 10.1186/s40623-020-01172-8
- 748 Matsuzawa, T., Hirose, H., Shibazaki, B., & Obara, K. (2010). Modeling short- and  
749 long-term slow slip events in the seismic cycles of large subduction earthquakes. *J.*  
750 *Geophys. Res.*, *115*, B12301. doi: 10.1029/2010JB007566
- 751 Matsuzawa, T., Obara, K., & Maeda, T. (2009). Source duration of deep very low  
752 frequency earthquakes in western Shikoku, Japan. *J. Geophys. Res.*, *114*, B00A11.  
753 doi: 10.1029/2008JB006044
- 754 Maury, J., Ide, S., Cruz-Atienza, V. M., Kostoglodov, V., Gonzalez-Molina, G., &  
755 Prez-Campos, X. (2016). Comparative study of tectonic tremor locations: Char-  
756 acterization of slow earthquakes in Guerrero, Mexico. *J. Geophys. Res.*, *121*(7),  
757 5136–5151. doi: 10.1002/2016JB013027
- 758 McCrory, P. A., Blair, J. L., Waldhauser, F., & Oppenheimer, D. H. (2012). Juan de  
759 Fuca slab geometry and its relation to Wadati-Benioff zone seismicity. *J. Geophys.*  
760 *Res.*, *117*(B9), B09306. doi: 10.1029/2012JB009407
- 761 Michel, S., Avouac, J.-P., Lapusta, N., & Jiang, J. (2017). Pulse-like partial ruptures  
762 and high-frequency radiation at creeping-locked transition during megathrust  
763 earthquakes. *Geophys. Res. Lett.*, *44*. doi: 10.1002/2017GL074725
- 764 Michel, S., Gualandi, A., & Avouac, J.-P. (2019). Similar scaling laws for earth-  
765 quakes and Cascadia slow-slip events. *Nature*, *574*(7779), 522–526. doi: 10.1038/  
766 s41586-019-1673-6
- 767 Miller, M. M., Melbourne, T., Johnson, D. J., & Sumner, W. Q. (2002). Periodic  
768 slow earthquakes from the Cascadia subduction zone. *Science*, *295*(5564), 2423–  
769 2423. doi: 10.1126/science.1071193
- 770 Nicholson, T., Bostock, M., & Cassidy, J. F. (2005). New constraints on subduction  
771 zone structure in northern Cascadia. *Geophys. J. Intern.*, *161*(3), 849–859. doi: 10  
772 .1111/j.1365-246X.2005.02605.x
- 773 Noda, H., Dunham, E. M., & Rice, J. R. (2009). Earthquake ruptures with thermal  
774 weakening and the operation of major faults at low overall stress levels. *J. Geo-*  
775 *phys. Res.*, *114*, B07302. doi: 10.1029/2008JB006143
- 776 Obara, K. (2002). Nonvolcanic deep tremor associated with subduction in southwest  
777 Japan. *Science*, *296*(5573), 1679–1681. doi: 10.1126/science.1070378
- 778 Obara, K. (2010). Phenomenology of deep slow earthquake family in southwest  
779 Japan: Spatiotemporal characteristics and segmentation. *J. Geophys. Res.*, *115*,  
780 B00A25. doi: 10.1029/2008JB006048
- 781 Obara, K. (2012). Depth-dependent mode of tremor migration beneath Kii Penin-  
782 sula, Nankai subduction zone. *Geophys. Res. Lett.*. doi: 10.1029/2012GL051420
- 783 Obara, K., Hirose, H., Yamamizu, F., & Kasahara, K. (2004). Episodic slow slip  
784 events accompanied by non-volcanic tremors in southwest Japan subduction zone.  
785 *Geophys. Res. Lett.*, *31*, L23602. doi: 10.1029/2004GL020848
- 786 Obara, K., & Sekine, S. (2009). Characteristic activity and migration of episodic  
787 tremor and slow-slip events in central Japan. *Earth Planets and Space*, *61*(7),  
788 853–862.
- 789 Ochi, T., Itaba, S., Koizumi, N., Takahashi, M., Matsumoto, N., Kitagawa, Y., ...  
790 Shiomi, K. (2016). *Short-term slow slip events in the Tokai area, the Kii Penin-*  
791 *sula and the Shikoku District, Japan (from May 2015 to October 2015)* (Report of  
792 the Coordinating Committee for Earthquake Prediction No. 95).
- 793 Peng, Y., & Rubin, A. M. (2016). High-resolution images of tremor migrations be-  
794 neath the Olympic Peninsula from stacked array of arrays seismic data. *Geochem.*,  
795 *Geophys.*, *Geosyst.*, *17*(2), 587–601. doi: 10.1002/2015GC006141
- 796 Peng, Y., & Rubin, A. M. (2017). Intermittent tremor migrations beneath Guerrero,  
797 Mexico, and implications for fault healing within the slow slip zone. *Geophys. Res.*  
798 *Lett.*, *44*(2), 2016GL071614. doi: 10.1002/2016GL071614
- 799 Peng, Y., & Rubin, A. M. (2018). Simulating short-term evolution of slow slip in-  
800 fluenced by fault heterogeneities and tides. *Geophys. Res. Lett.*, *45*(19), 10,269–  
801

- 10,278. doi: 10.1029/2018GL078752
- 802 Peng, Y., Rubin, A. M., Bostock, M. G., & Armbruster, J. G. (2015). High-  
803 resolution imaging of rapid tremor migrations beneath southern Vancouver Island  
804 using cross-station cross correlations. *J. Geophys. Res.*, *120*(6), 4317–4332. doi:  
805 10.1002/2015JB011892
- 806 Romanet, P., Bhat, H. S., Jolivet, R., & Madariaga, R. (2018). Fast and slow slip  
807 events emerge due to fault geometrical complexity. *Geophys. Res. Lett.*, *45*(10),  
808 4809–4819. doi: 10.1029/2018GL077579
- 809 Rousset, B., Campillo, M., Lasserre, C., Frank, W. B., Cotte, N., Walpersdorf,  
810 A., ... Kostoglodov, V. (2017). A geodetic matchedfilter search for slow  
811 slip with application to the Mexico subduction zone. *J. Geophys. Res.* doi:  
812 10.1002/2017JB014448
- 813 Royer, A. A., Thomas, A. M., & Bostock, M. G. (2015). Tidal modulation and  
814 triggering of low-frequency earthquakes in northern Cascadia. *J. Geophys. Res.*,  
815 *120*(1), 384–405. doi: 10.1002/2014JB011430
- 816 Rubin, A. M. (2008). Episodic slow slip events and rate-and-state friction. *J. Geo-  
817 phys. Res.*, *113*, B11414. doi: 10.1029/2008JB005642
- 818 Rubin, A. M. (2011). Designer friction laws for bimodal slow slip propagation  
819 speeds. *Geochem., Geophys., Geosyst.*, *12*, Q04007. doi: 10.1029/2010GC003386
- 820 Rubin, A. M., & Armbruster, J. G. (2013). Imaging slow slip fronts in Cascadia  
821 with high precision cross-station tremor locations. *Geochem., Geophys., Geosyst.*,  
822 *14*, 5371–5392. doi: 10.1002/2013GC005031
- 823 Savard, G., & Bostock, M. G. (2015). Detection and location of lowfrequency earth-  
824 quakes using crossstation correlation. *Bull. Seis. Soc. Amer.*, *105*(4), 2128–2142.  
825 doi: 10.1785/0120140301
- 826 Schmidt, D. A., & Gao, H. (2010). Source parameters and time-dependent slip dis-  
827 tributions of slow slip events on the Cascadia subduction zone from 1998 to 2008.  
828 *J. Geophys. Res.*, *115*, B00A18. doi: 10.1029/2008JB006045
- 829 Segall, P., & Rice, J. R. (1995). Dilatancy, compaction, and slip instability of a  
830 fluid-infiltrated fault. *J. Geophys. Res.*, *100*(B11), 22155–22171. doi: 10.1029/  
831 95JB02403
- 832 Segall, P., Rubin, A. M., Bradley, A. M., & Rice, J. R. (2010). Dilatant strengthen-  
833 ing as a mechanism for slow slip events. *J. Geophys. Res.*, *115*, B12305. doi: 10  
834 .1029/2010JB007449
- 835 Sekine, S., Hirose, H., & Obara, K. (2010). Along-strike variations in short-term  
836 slow slip events in the southwest Japan subduction zone. *J. Geophys. Res.*, *115*,  
837 B00A27. doi: 201010.1029/2008JB006059
- 838 Shelly, D. R. (2010). Migrating tremors illuminate complex deformation beneath  
839 the seismogenic San Andreas fault. *Nature*, *463*(7281), 648–652. doi: 10.1038/  
840 nature08755
- 841 Shelly, D. R. (2017). A 15year catalog of more than 1 million low-frequency earth-  
842 quakes: Tracking tremor and slip along the deep San Andreas Fault. *J. Geophys.  
843 Res.*, *122*(5), 3739–3753. doi: 10.1002/2017JB014047
- 844 Shelly, D. R., Beroza, G. C., Ide, S., & Nakamura, S. (2006). Low-frequency earth-  
845 quakes in Shikoku, Japan, and their relationship to episodic tremor and slip. *Na-  
846 ture*, *442*(7099), 188–191. doi: 10.1038/nature04931
- 847 Shibazaki, B., & Iio, Y. (2003). On the physical mechanism of silent slip events  
848 along the deeper part of the seismogenic zone. *Geophys. Res. Lett.*, *30*(9), 1489.  
849 doi: 10.1029/2003GL017047
- 850 Shibazaki, B., & Shimamoto, T. (2007). Modelling of short-interval silent slip  
851 events in deeper subduction interfaces considering the frictional properties at the  
852 unstable-stable transition regime. *Geophys. J. Intern.*, *171*(1), 191–205. doi:  
853 10.1111/j.1365-246X.2007.03434.x
- 854 Skarbek, R. M., Rempel, A. W., & Schmidt, D. A. (2012). Geologic heterogeneity
- 855

- 856 can produce aseismic slip transients. *Geophys. Res. Lett.*, *39*(21), L21306. doi: 10  
857 .1029/2012GL053762
- 858 Sun, W.-F., Peng, Z., Lin, C.-H., & Chao, K. (2015). Detecting deep tectonic tremor  
859 in Taiwan with a dense array. *Bull. Seis. Soc. Amer.*, *105*(3), 1349–1358. doi: 10  
860 .1785/0120140258
- 861 Supino, M., Poiata, N., Festa, G., Vilotte, J. P., Satriano, C., & Obara, K. (2020).  
862 Self-similarity of low-frequency earthquakes. *Scientific Reports*, *10*(1), 6523. doi:  
863 10.1038/s41598-020-63584-6
- 864 Takeo, A., Idehara, K., Iritani, R., Tonegawa, T., Nagaoka, Y., Nishida, K., ...  
865 Obara, K. (2010). Very broadband analysis of a swarm of very low frequency  
866 earthquakes and tremors beneath Kii Peninsula, SW Japan. *Geophys. Res. Lett.*,  
867 *37*, L06311. doi: 10.1029/2010GL042586
- 868 Thomas, A. M., Beeler, N. M., Bletery, Q., Burgmann, R., & Shelly, D. R. (2018).  
869 Using low-frequency earthquake families on the San Andreas Fault as deep creep-  
870 meters. *J. Geophys. Res.*, *123*(1), 457–475. doi: 10.1002/2017JB014404
- 871 Thomas, A. M., Beroza, G. C., & Shelly, D. R. (2016). Constraints on the source  
872 parameters of low-frequency earthquakes on the San Andreas Fault. *Geophys. Res.*  
873 *Lett.*, *43*(4), 1464–1471. doi: 10.1002/2015GL067173
- 874 Thomas, T. W., Vidale, J. E., Houston, H., Creager, K. C., Sweet, J. R., & Ghosh,  
875 A. (2013). Evidence for tidal triggering of high-amplitude rapid tremor reversals  
876 and tremor streaks in northern Cascadia. *Geophys. Res. Lett.*, *40*(16), 4254–4259.  
877 doi: 10.1002/grl.50832
- 878 Tu, Y., & Heki, K. (2017). Decadal modulation of repeating slow slip event  
879 activity in the southwestern Ryukyu Arc possibly driven by rifting episodes  
880 at the Okinawa Trough. *Geophys. Res. Lett.*, *44*(18), 9308–9313. doi:  
881 10.1002/2017GL074455
- 882 UNAVCO. (2005). *Plate Boundary Observatory, EarthScope. Dataset / seismic net-*  
883 *work.*
- 884 University of Washington. (1963). *Pacific Northwest Seismic Network. International*  
885 *Federation of Digital Seismograph Networks. Dataset / seismic network.* doi:  
886 <https://doi.org/10.7914/SN/UW>
- 887 Vaca, S., Valle, M., Nocquet, J.-M., Battaglia, J., & Rgnier, M. (2018). Recurrent  
888 slow slip events as a barrier to the northward rupture propagation of the 2016  
889 Pedernales earthquake (Central Ecuador). *Tectonophysics*, *724-725*, 80–92. doi:  
890 10.1016/j.tecto.2017.12.012
- 891 Walter, J. I., Schwartz, S. Y., Protti, M., & Gonzalez, V. (2013). The synchronous  
892 occurrence of shallow tremor and very low frequency earthquakes offshore of  
893 the Nicoya Peninsula, Costa Rica. *Geophys. Res. Lett.*, *40*(8), 1517–1522. doi:  
894 10.1002/grl.50213
- 895 Wang, J., Dennise C. Templeton, & Harris, D. B. (2015). Discovering new  
896 events beyond the catalogue application of empirical matched field processing  
897 to Salton Sea geothermal field seismicity. *Geophys. J. Intern.*, *203*(1), 22–32. doi:  
898 10.1093/gji/ggv260
- 899 Wech, A. G., & Bartlow, N. M. (2014). Slip rate and tremor genesis in Cascadia.  
900 *Geophys. Res. Lett.*, *41*(2), 392–398. doi: 10.1002/2013GL058607
- 901 Wech, A. G., Creager, K. C., & Melbourne, T. I. (2009). Seismic and geodetic con-  
902 straints on Cascadia slow slip. *J. Geophys. Res.*, *114*, B10316. doi: 10.1029/  
903 2008JB006090
- 904 Wei, M., Kaneko, Y., Shi, P., & Liu, Y. (2018). Numerical modeling of dynamically  
905 triggered shallow slow slip events in New Zealand by the 2016 Mw 7.8 Kaikoura  
906 earthquake. *Geophys. Res. Lett.*, *45*(10), 4764–4772. doi: 10.1029/2018GL077879
- 907 Yabe, S., Baba, S., Tonegawa, T., Nakano, M., & Takemura, S. (2021). Seismic  
908 energy radiation and along-strike heterogeneities of shallow tectonic tremors  
909 at the Nankai Trough and Japan Trench. *Tectonophysics*, *800*, 228714. doi:

910 10.1016/j.tecto.2020.228714

911 Yamashita, Y., Yakiwara, H., Asano, Y., Shimizu, H., Uchida, K., Hirano, S., ...

912 Obara, K. (2015). Migrating tremor off southern Kyushu as evidence for  
913 slow slip of a shallow subduction interface. *Science*, *348*(6235), 676–679. doi:

914 10.1126/science.aaa4242

915 Zheng, G., & Rice, J. R. (1998). Conditions under which velocity-weakening friction  
916 allows a self-healing versus a cracklike mode of rupture. *Bull. Seis. Soc. Amer.*,

917 *88*(6), 1466–1483.